

Characteristic Phase Transition of $[C_5H_5NH]SbBr_4$ Having a Hypervalent Bond Studied by Single Crystal X-Ray Diffraction and ^2H NMR

Koji Yamada,* Takuya Tsuda, Christian Holst, Tsutomu Okuda, Helmut Ehrenberg,† Ingrid Svoboda,† Hans-Georg Krane,†† and Hartmut Fuess†

Department of Chemistry, Graduate School of Science, Hiroshima University, Kagamiyama, Higashi-Hiroshima 739-8526

† Institute for Materials Science, Darmstadt University of Technology, Petersenstrasse 23, Darmstadt D-64287, Germany

†† Institute for Mineralogy and Petrology, University of Bonn, Poppelsdorfer Schloss, Bonn D-53115, Germany

(Received August 2, 2000)

A characteristic second-order phase transition (T_{tr} = 251 K) of pyridinium tetrabromoantimonate(III) having hypervalent bonds was studied by means of the single-crystal X-ray diffraction and ^2H NMR. The $SbBr_4^-$ anion in $[C_5H_5NH]SbBr_4$ forms an infinite zigzag chain of irregular $SbBr_6$ octahedra by sharing two edges. This $SbBr_4^-$ anion has C_2 symmetry on the Sb atom perpendicular to the infinite chain. Hence, each octahedron has one symmetric *trans* Br(2)–Sb–Br(2) bond and two asymmetric *trans* Br(1)–Sb···Br(2) above T_{tr}. However, a structural refinement on Phase II at 110 K revealed a characteristic deformation of one symmetric *trans* Br(2)–Sb–Br(2) bond to an asymmetric one, i.e., one Sb–Br(2) bond becomes shorter by 0.113(2) Å and the other bond located at the *trans* position becomes longer by 0.129(2) Å. The structural refinement and the ^2H NMR on an N-deuterated analog suggest that the N–H···Br hydrogen bond stabilizes the asymmetric *trans* Br–Sb···Br bond.

Static and dynamic structures of halocomplexes of main-group elements, such as Sn(II), Ge(II), and Sb(III), have been extensively studied because they showed characteristic phase transitions induced by raising the temperature or applying pressure.[1,2] In some cases the electronic[3,4] or ionic conductivity[5,6] changes drastically at the phase-transition temperatures. The $SbBr_4^-$ anion in pyridinium tetrabromoantimonate(III), $[C_5H_5NH]SbBr_4$, forms an infinite chain of an irregular $SbBr_6$ octahedron sharing two edges. Since the 5*s*-orbital of Sb^{3+} is occupied by a lone pair, only three *p*-orbitals are mainly used for the bondings with six ligands. This situation is called a hypervalent state of the central atom because there is more than an octet of electrons around the central atom.[1,7] Although this orbital-deficient feature appears in three orthogonal directions, the situation is essentially the same as a bonding found in a linear I_3^- anion where a three-center four-electron (3c-4e) bond has been proposed by Pimentel.[8] Therefore, a 3c-4e bond is a one dimensional model of the hypervalent bond. It should be noted that a linear X–M–X (X: halogen) bond formed by a 3c-4e bond tends to deform into an asymmetric X–M···X one depending upon the electrostatic environment. In our previous paper on $[C_5H_5NH]SbBr_4$, we reported an extremely large splitting of the NQR signals below 253 K for the ^{81}Br assigned to the *trans* Br–Sb–Br. Although the splitting at 77 K reached ca. 84% of the ^{81}Br NQR frequency in Phase I, the mean frequency remained almost constant.[9] These observations suggested that more valence electrons of the *trans* Br–Sb–Br bond being localized on one Br atom resulted in a considerably asymmetric Br–Sb···Br bond at 77 K. Powder X-ray diffraction at 116 K on $[C_5H_5NH]SbBr_4$ also supported a large deformation of the anion. Furthermore, ^2H NMR measurements suggested that the gradual quenching of the large librational amplitude on the pyridinium ring stabilized the asymmetric *trans* Br–Sb···Br bond below T_{tr}, forming an N–H···Br hydrogen bond.[10]

In this report the structural change of $[C_5H_5NH]SbBr_4$ from Phase I to II, including a dynamical aspect of the N–H···Br hydrogen bond, is discussed based on the hypervalent nature of Sb(III).

Experimental

Sample Preparation. Pyridinium tetrabromoantimonate(III) was prepared by crystallization from a HBr solution containing stoichiometric amounts of Sb_2O_3 and pyridinium bromide. Pale-yellow crystals were filtered off and dried *in vacuo*. N-deuterated $[C_5H_5N^2H]SbBr_4$ was obtained by refluxing the hydrated analog in an acidic ^2H_2O solution. A large single crystal of $[C_5H_5N^2H]SbBr_4$ was grown by means of a Bridgman technique in a sealed glass tube. A slight amount of ^2HBr was added into the sample tube in order to prevent the formation of the other high-temperature phase, which was normally obtained from the melt.

Synchrotron Diffraction on a Powder Sample. The high-resolution powder diffraction data at 175 K were recorded for the

2θ range from 6 to 60° in steps of 0.006° on a flat sample in reflection geometry at beam line B2 of HASYLAB, Germany. A wavelength of 1.3738(1) Å was selected by a Ge(111) double-crystal monochromator and an additional Ge(111) analysing crystal between the sample and a NaI-scintillation counter.

X-Ray Diffraction on a Single Crystal. A single crystal (0.1 × 0.1 × 0.15 mm) of [C_5H_5NH]$SbBr_4$ was mounted on a Mac Science DP2030 imaging-plate diffractometer with monochromatized Mo $K\alpha$ radiation ($\lambda = 0.71069$ Å). X-ray measurements were performed at 295, 170 and 110 K with an Oxford Cryostream cooler. Intensity measurements were performed using the oscillation method at an oscillation width of 3° with an exposure time of 360 s per photograph. Sixty photographs were taken at each temperature. The unit-cell parameters were determined using all observed reflections over the range of $2\theta = 4.8$–$54.9°$. Below T_{tr} each reflection spot split into two, suggesting two large fragments. However, about half of the observed reflections could be successfully indexed as a triclinic lattice, which agreed well with those from our synchrotron diffraction. The intensity data were corrected for Lorentz and polarization effects. φ-Scan like empirical absorption corrections were performed on the intensity data. The structures were solved by DIRDIF92[11] and expanded using difference Fourier techniques. All of the calculations were performed using a "teXsan" crystallographic software package of Molecular Structure Corporation.[12] The nonhydrogen atoms were refined anisotropically. Hydrogen atoms were included in the structure-factor calculation, but were not refined. Crystallographic data and details of the structural determinations for [C_5H_5NH]$SbBr_4$ are summarized in Table 1. Crystallographic data have been deposited as document No. 74005 at the Office of the Editor of Bull Chem. Soc. Jpn. and also deposited at the CCDC, 12 Union Road, Cambridge CB2 1EZ, UK and copies can be obtained on request, free of charge, by quoting the publication and deposition numbers 151205–151207.

^{2}H NMR Measurements. ^{2}H NMR powder spectra were observed by a homebuilt spectrometer using a solid echo technique, followed by a Fourier transformation of the echo signal. The typical pulse length was 3 μs for an 8 mm diameter sample tube. Single-crystal measurements were performed using a similar probe with a goniometer head. A single crystal having dimensions of ca. 5 × 5 × 5 mm was packed into a cubic crystal holder (10 mm) and was rotated around the axis normal to the external field. The quadrupole splittings due to $\Delta m = \pm 1$ transitions were observed as a function of the crystal rotation. Three orthogonal rotations, denoted as X, Y, and Z-rotation, were performed.

Results and Discussion

DTA. Figure 1 shows DTA curves for [C_5H_5NH]$SbBr_4$ and N-deuterated analog, [$C_5H_5N^2H$]$SbBr_4$. The phase-transition temperatures were determined to be 251(1) K and 247(1) K for [C_5H_5NH]$SbBr_4$ and N-deuterated analog, respectively. The phase-transition temperature on [C_5H_5NH]$SbBr_4$ in this work agreed well with that previously reported by the ^{81}Br NQR (T_{tr} = 253 K). In spite of the drastic ^{81}Br NQR splitting below T_{tr}, only slight baseline shifts were observed on these DTA curves. These thermal behaviors suggest that the phase transition is a displacive type other than an order-disorder type. Hereafter, these two phases are abbreviated as Phase I and Phase II from the high-temperature side.

Crystal Structures of [C_5H_5NH]$SbBr_4$ at 295, 170, and 110 K. The crystal structure of [C_5H_5NH]$SbBr_4$ at Phase I

Table 1. Crystallographic Data for [C_5H_5NH]$SbBr_4$ at 295, 170 and 110 K

Temperature/K	295(1)	170(2)	110(2)
Formula weight	521.48	521.48	521.48
Diffractometer	Mac Science DIP2030	Mac Science DIP2030	Mac Science DIP2030
Wavelength/Å	0.71069	0.71069	0.71069
Crystal size/mm	0.10 × 0.10 × 0.15	0.10 × 0.10 × 0.15	0.10 × 0.10 × 0.15
Crystal system	monoclinic	triclinic	triclinic
a/Å	11.8370(8)	7.6350(4)	7.6080(3)
b/Å	13.0450(9)	8.7120(7)	8.6780(6)
c/Å	7.6990(3)	8.7980(8)	8.7880(6)
α/deg	90.00	95.135(3)	95.013(3)
β/deg	93.852(4)	90.404(3)	89.889(4)
γ/deg	90.00	94.629(5)	95.134(3)
Volume of unit cell/Å^3	1186.1(1)	582.90(7)	575.66(5)
Space group	$C2/c$ (No. 15)	$P\bar{1}$ (No. 2)	$P\bar{1}$ (No. 2)
Z Value	4	2	2
D_{calc}/g cm^{-3}	2.920	2.981	3.008
μ /mm^{-1}	15.786	16.117	16.264
No. of independent reflections	1352	2483	2499
Least square refinement	Full Matrix	Full Matrix	Full Matrix
Weight method	calc	calc	calc
Calc w=1/[$\sigma^2(F_o) + a\|F_o\|^2$]	$a = 0.002$	0.01	0.01
Reflections used in L.S.	1198	2160	2254
Data reduction cut-off	$> 2.0\,\sigma(I)$	$> 2.0\,\sigma(I)$	$> 2.0\,\sigma(I)$
L. S. Parameters	53	100	100
R ($> 2.0\sigma$)	0.0517	0.1091	0.1046
R_w ($> 2.0\sigma$)	0.1010	0.1662	0.1725
Max shift/e.s.d	0.013	0.007	0.010
Goodness of fit	1.722	1.555	1.638

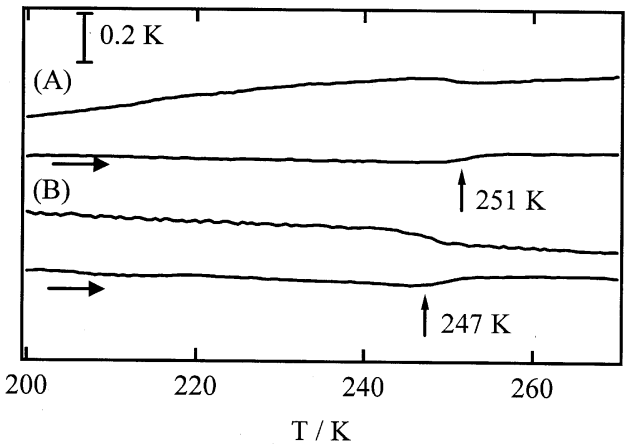

Fig. 1. DTA curves for (A) $[C_5H_5NH]SbBr_4$ and (B) $[C_5H_5N^2H]SbBr_4$.

had already been reported in the literature.[13] However, in order to examine the structural change from Phase I to Phase II in detail, X-ray diffraction measurements on a single crystal were performed at three different temperatures. Table 2 summarizes the positional and thermal parameters at 295, 170 and 110 K. The bond lengths and angles and the hydrogen bonding geometry at three different temperatures are summarized in Tables 3 and 4. Figure 2 shows the packing of the anions and cations projected parallel to the infinite chain of the $SbBr_4^-$ anion. The most remarkable structural difference between Phases I and II is seen on the geometry of the N–H···Br hydrogen bonding as shown in Fig. 3.

Phase I. In the anionic sublattice each Sb atom is surrounded by six Br atoms, forming an irregular octahedron. An infinite zigzag chain is formed by sharing two edges of the octahedron. Since the pyridinium cation and the Sb atom are located on the C_2 axis in Phase I, two hydrogen bonds N–H···Br(2) are formed symmetrically, as shown in Figs. 2(A) and 3(A). Only two ^{81}Br NQR signals assigned to a terminal Br(1) and a bridging Br(2) are consistent with this structure. The ^{81}Br NQR frequency of the terminal Br(1) was reported to be ca. 120 MHz, which was about two-times larger than that of the bridging one in Phase I. These findings from the X-ray and NQR suggest that the negative charges of the anionic sublattice concentrate on the two bridging Br(2) atoms forming a symmetric *trans* Br(2)–Sb(1)–Br(2) bond. The bond lengths in this irregular octahedron show a characteristic feature of the hypervalent element, i.e., a short Sb–Br bond lengthens the Sb–Br bond at

Table 2. Positional Parameters and Equivalent Isotropic Thermal Parameters for $[C_5H_5NH]SbBr_4$ at (A) 295, (B) 170 and (C)110 K

(A) atom	x	y	z	U_{iso}/Å^{2} a)
Sb(1)	0.0000	0.08636(7)	0.2500	2.71(2)
Br(1)	0.13255(9)	0.22005(10)	0.1272(2)	4.52(3)
Br(2)	0.1393(1)	0.08970(10)	0.5619(2)	4.26(3)
N(1)	0.5000	0.181(1)	0.2500	7.5(5)
C(1)	0.412(1)	0.132(1)	0.306(2)	6.1(4)
C(2)	0.408(1)	0.031(1)	0.303(2)	6.5(4)
C(3)	0.5000	−0.023(2)	0.2500	6.0(5)
(B)				
Sb(1)	−0.2528(1)	−0.0891(1)	0.0856(1)	1.61(3)
Br(1)	−0.1252(3)	−0.3528(2)	0.0734(2)	2.63(4)
Br(2)	−0.3750(2)	−0.1055(2)	0.3567(2)	2.65(4)
Br(3)	−0.5535(2)	−0.2305(2)	−0.0482(2)	2.47(4)
Br(4)	0.0788(2)	0.0443(2)	0.2308(2)	2.32(4)
N(1)	0.781(3)	0.298(2)	0.667(2)	3.5(4)
C(1)	0.830(3)	0.260(2)	0.518(3)	3.4(5)
C(2)	0.814(3)	0.360(3)	0.416(3)	3.7(5)
C(3)	0.750(3)	0.510(3)	0.460(3)	3.5(5)
C(4)	0.707(3)	0.539(2)	0.607(3)	4.0(5)
C(5)	0.720(2)	0.434(3)	0.713(2)	3.9(5)
(C)				
Sb(1)	−0.2534(1)	−0.0892(1)	0.0862(1)	0.97(3)
Br(1)	−0.1244(2)	−0.3528(2)	0.0712(2)	1.55(4)
Br(2)	−0.3759(2)	−0.1093(2)	0.3583(2)	1.60(4)
Br(3)	−0.5525(2)	−0.2316(2)	−0.0470(2)	1.49(3)
Br(4)	0.0828(2)	0.0433(2)	0.2305(2)	1.36(3)
N(1)	0.788(2)	0.298(2)	0.663(2)	2.0(3)
C(1)	0.831(2)	0.258(2)	0.518(2)	1.6(3)
C(2)	0.811(2)	0.360(2)	0.411(2)	1.9(3)
C(3)	0.749(2)	0.507(2)	0.455(2)	1.9(4)
C(4)	0.703(3)	0.538(2)	0.608(3)	2.5(4)
C(5)	0.721(2)	0.433(2)	0.712(2)	1.8(3)

a) $U_{iso} = 1/3(\Sigma_i\Sigma_j U_{ij} a_i^* a_j^* \mathbf{a}_i \cdot \mathbf{a}_j)$

Table 3. Selected Bond Distances and Angles in $[C_5H_5NH]SbBr_4$ at 295, 170 and 110 K

Bond/Å or Angle/degree	295 K	Bond/Å or Angle/degree	170 K	110 K
Sb(1)–Br(1)	2.569(1)	Sb(1)–Br(1)	2.560(2)	2.561(2)
		Sb(1)–Br(2)	2.580(2)	2.580(2)
Sb(1)–Br(2)	2.821(1)	Sb(1)–Br(3)	2.724(2)	2.708(2)
		Sb(1)–Br(4)	2.934(2)	2.950(2)
Sb(1)–Br(2)^{i}	3.227(1)	Sb(1)–Br(3)^{iii}	3.297(2)	3.310(2)
		Sb(1)–Br(4)^{iv}	3.135(2)	3.111(2)
Br(1)–Sb(1)–Br(1)^{ii}	94.46(7)	Br(1)–Sb(1)–Br(2)	94.57(7)	94.55(6)
Br(2)–Sb(1)–Br(2)^{ii}	178.23(6)	Br(3)–Sb(1)–Br(4)	176.46(6)	175.79(5)
Br(1)–Sb(1)–Br(2)	172.65(3)	Br(1)–Sb(1)–Br(3)^{iii}	170.85(6)	170.27(6)
		Br(2)–Sb(1)–Br(4)^{iv}	174.62(7)	175.23(6)

Symmetry codes for $C2/c$: (i) $-x, -y, 1-z$, (ii) $-x, y, 1/2-z$
Symmetry codes for $P\bar{1}$: (iii) $-1-x, -y, -z$, (iv) $-x, -y, -z$

Table 4. Hydrogen-bonding Geometry at 295, 170 and 110 K

Temperature/K	D–H···A	D–H/Å	H··· A/Å	D···A/Å	< D–H···A/degree
295	N^{i}–H···Br(2)	0.96	3.04	3.75(1)	132
170	N^{ii}–H···Br(4)	0.96	2.64	3.44(1)	142
110	N^{ii}–H···Br(4)	0.96	2.64	3.41(1)	141

Symmetry code for $C2/c$: (i) $-1/2+x, 1/2-y, -1/2+z$
Symmetry code for $P\bar{1}$: (ii) $1-x, -y, 1-z$

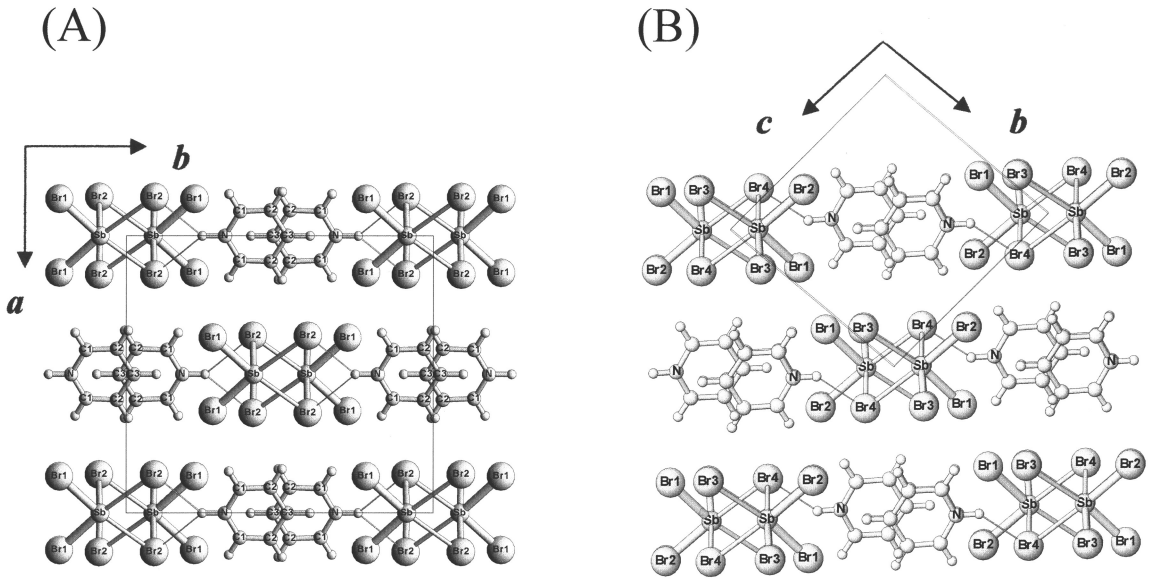

Fig. 2. Projection of $[C_5H_5NH]SbBr_4$ structure parallel to the infinite anionic chains. (A) Phase I at 295 K and (B) Phase II at 110 K.

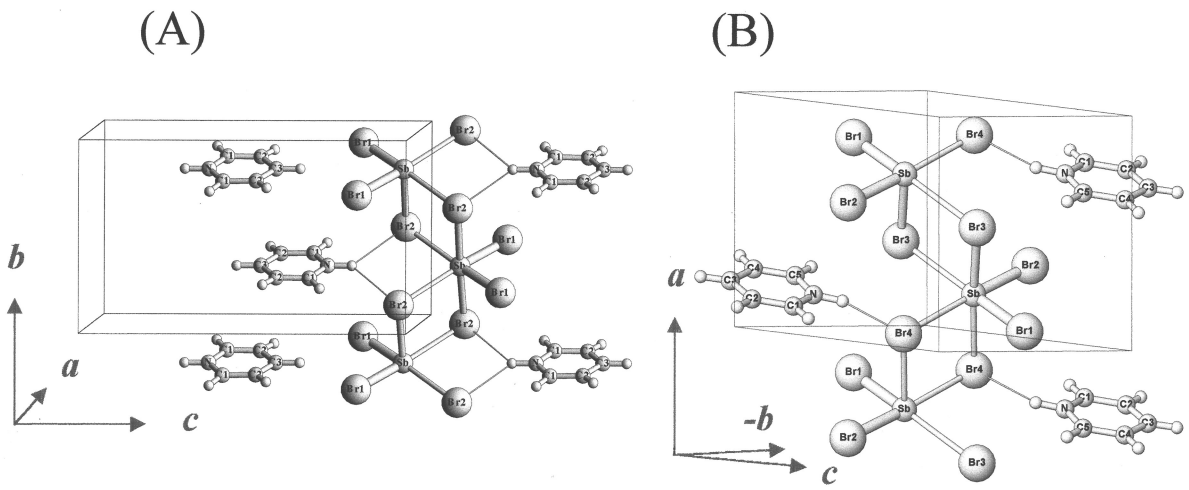

Fig. 3. Comparison between structures at 295 K (Phase I) and 110 K (Phase II). (A) Two hydrogen bonds N−H···Br(2) and *trans* Br(2)−Sb−Br(2) are formed symmetrically due to the crystal symmetry at Phase I. (B) Hydrogen bond is formed between only Br(4) and N−H due to the rotation and the displacement of the cation at Phase II.

the *trans* position or *vice versa*. On the other hand, the cationic position could be determined without introducing any orientational disorder. This finding is consistent with the DTA and ^{2}H NMR measurements in which a librational oscillation having a large amplitude was suggested.[10]

Phase II. The phase transition into Phase II with decreasing temperature was accompanied by the appearance of additional reflections and the splitting of some reflections in the powder diffraction pattern. This powder pattern from synchrotron radiation could be indexed based on a triclinic cell with a_{II} = 7.62635(13) Å, b_{II} = 8.71631(13) Å, c_{II} = 8.78390(13) Å, α_{II} = 95.167(1)°, β_{II} = 90.367(1)°, γ_{II} = 94.648(1)° at 175 (1) K.

The cell of Phase II is derived from the monoclinic cell of Phase I by the following transformation:

$$\begin{aligned} \boldsymbol{a}_{\mathbf{II}} &= \boldsymbol{c}_{\mathbf{I}}, \\ \boldsymbol{b}_{\mathbf{II}} &= (1/2)(\boldsymbol{a}_{\mathbf{I}} - \boldsymbol{b}_{\mathbf{I}}), \\ \boldsymbol{c}_{\mathbf{II}} &= (1/2)(\boldsymbol{a}_{\mathbf{I}} + \boldsymbol{b}_{\mathbf{I}}), \end{aligned} \quad (1)$$

with $V_{II} \approx (1/2)V_I$ and additional distortion. However, a structural determination on Phase II directly from the powder data was not successful due to a very pronounced preferred orientation of our powder sample.

On the other hand, in our single-crystal X-ray diffraction measurement, the single crystal could not be maintained below T_{tr}. In most cases, single crystals broke into two large fragments below T_{tr}. However, one set of reflections could be indexed based on the triclinic cell, which was determined by a synchrotron experiment on a powder sample. Although the R parameters at Phase II are still high, probably due to the overlapping two set of reflections, a characteristic distortion of the hypervalent bond can be clearly demonstrated, as shown in Figs. 2, 3 and 4. Figure 3 shows the geometrical change of the hydrogen bond from Phase I to II. The *trans* Br(2)–Sb(1)–Br(2) bond in Phase I is symmetric and, hence, two hydrogen bonds N–H···Br(2) are formed symmetrically. However, only one N–H···Br(4) hydrogen bond is formed in Phase II due to the translational and rotational shift of the cation. Figure 4 plots the Sb–Br bond length against temperature, where dotted lines are drawn continuously by eyes because the ^{81}Br NQR splitting below T_{tr} shows the feature of a second-order phase transition. Figure 4 shows the characteristic feature of the 3c-4e bond, especially on the *trans* Br(3)–Sb–Br(4). That is, a symmetric *trans* Br–Sb–Br bond deforms asymmetrically, Br(3)–Sb···Br(4), suggesting that the excess electrons on the 3c-4e bond are localized on Br(4). The formation of the N–H···Br(4) hydrogen bond may contribute to stabilization of the asymmetric 3c-4e bond. This observation is consistent with our previous temperature dependence of the ^{81}Br NQR in which an extremely large splitting was observed below T_{tr}.

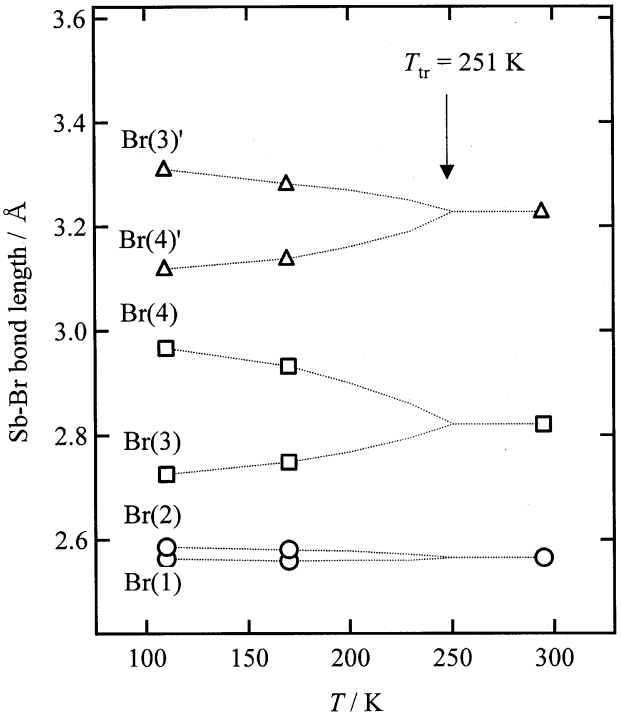

Fig. 4. Temperature dependence of the Sb-Br bond lengths corresponding to an irregular $SbBr_6$ octahedron. Dotted lines are drawn continuously by eyes because a second-order phase transition was confirmed at 251 K.

^{2}H NMR on Powdered Sample. Solid-state deuterium NMR is an especially valuable tool for studying the hydrogen-bond system because the quadrupole coupling constant reflects both static and dynamic structures of the hydrogen bond. Figure 5 shows the ^{2}H NMR spectra on the polycrystalline $[C_5H_5N^2H]SbBr_4$ at selective temperatures. $|e^2Qq_{ii}/h|$ and asymmetry parameter ($\eta = |(q_{yy} - q_{xx})/q_{zz}|$) evaluated from the spectra are plotted against temperature in Fig. 6, and are compared with the corresponding parameters for $[C_5{}^2H_5NH]SbBr_4$ (dotted lines).[10] Although the $|e^2Qq_{zz}/h|$ of $[C_5H_5N^2H]SbBr_4$ (191 kHz at 77 K) is about 10% larger than that of $[C_5{}^2H_5NH]SbBr_4$, their temperature behaviors are similar to each other. That is, $|e^2Qq_{zz}/h|$ and $|e^2Qq_{xx}/h|$ decrease continuously with increasing temperature, but $|e^2Qq_{yy}/h|$ remains almost constant over the whole temperature range studied. This temperature behavior could be explained by assuming a librational motion of the pyridinium ring about an axis normal to the ring. In the limit of the fast motion, the motional averaged efg components, q_{ii}', are expressed as follows:

$$\begin{aligned} q_{xx}' &= q_{xx}\cos^2\Theta + q_{zz}\sin^2\Theta, \\ q_{yy}' &= q_{yy}, \\ q_{zz}' &= q_{xx}\sin^2\Theta + q_{zz}\cos^2\Theta, \end{aligned} \quad (2)$$

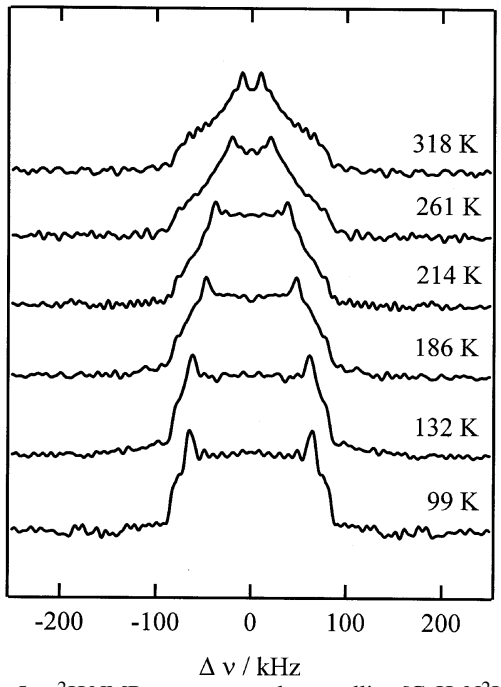

Fig. 5. ^{2}H NMR spectra on polycrystalline $[C_5H_5N^2H]SbBr_4$ at selected temperatures.

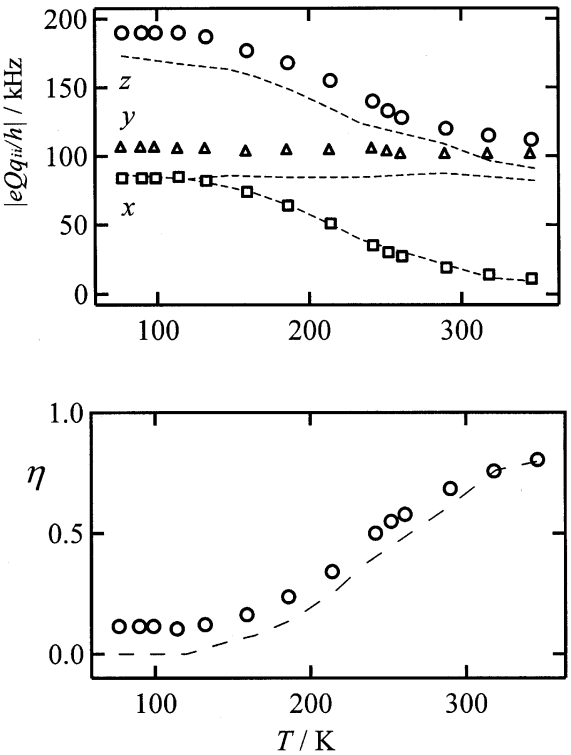

Fig. 6. Temperature dependence of the quadrupole coupling parameters, $|e^2Qq_{ii}/h|$ and η, for $[C_5H_5N^2H]SbBr_4$. Dotted lines correspond to $[C_5{}^2H_5NH]SbBr_4$.

where Θ is the root mean-square amplitude of the librational motion and q_{ii} are efg components at the rigid lattice. Figure 6 shows an interesting difference between $[C_5{}^2H_5NH]SbBr_4$ and $[C_5H_5N^2H]SbBr_4$ at a low-temperature region. The η assigned to the C–^{2}H decreases almost to zero at 77 K because no motions are excited at this temperature. On the other hand, the η assigned to the N–^{2}H is 11.6%, even at 77 K. These observations support the formation of the hydrogen bond N–^{2}H···Br(4), as shown in Fig. 3(B). Although the quadrupole coupling parameters are different from each other, partly due to the chemical bond and partly due to the hydrogen bond, the estimated Θ value at T_{tr} was 25(1)° for both deuterated analogs.

^{2}H NMR on a Single Crystal. Figure 7 shows typical single crystal spectra of ^{2}H NMR on $[C_5H_5N^2H]SbBr_4$. Only one pair of signals was observed at 285 K in spite of the monoclinic system. This is consistent with the fact that the N–^{2}H bond of the pyridinium cation is located on the C_2 axis in Phase I. Figure 8 plots the quadrupole splitting, $\Delta\nu$, between a pair of transitions (m_I =1 ↔ 0 and –1 ↔ 0) at 285 K. On the other hand, at 77 K, only one pair of signals was also expected from the space group ($P\bar{1}$, No.2), whereas two well-resolved doublets were observed, as shown in Figs. 7 and 9. These findings suggest that the single crystal changed to a twin structure below T_{tr}. We could not obtain a single crystal below T_{tr} similar to our X-ray diffraction. However, both rotational patterns at 285 K and 77 K could be analyzed by the Volkoff method. The

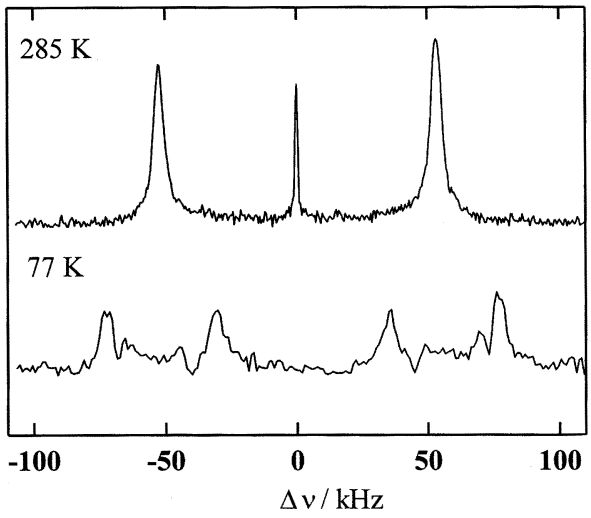

Fig. 7. Typical single crystal ^{2}H NMR spectra at 285 K (Phase I) and 77 K (Phase II). The sharp central signals at 285 K was assigned to ^2H_2O incorporated in to the crystal.

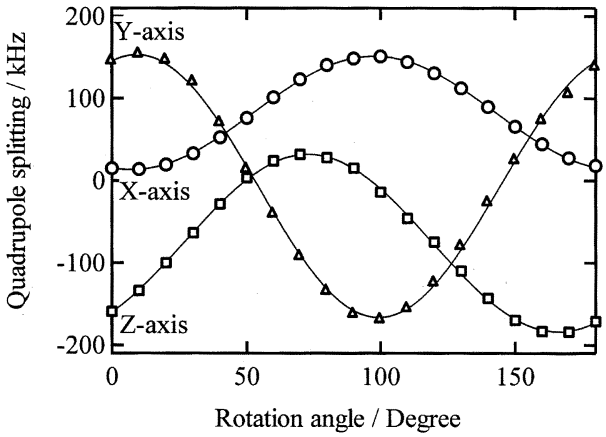

Fig. 8. ^{2}H NMR rotation pattern on $[C_5H_5N^2H]SbBr_4$ at 285 K. Quadrupole splitting between a pair of ^{2}H NMR transitions is plotted as a function of crystal rotation, ϕ.

splitting, $\Delta\nu$, was fitted to the function

$$\Delta\nu_i = A_i + B_i\cos^2\phi + C_i\sin^2\phi \quad (i = X, Y, \text{and } Z), \tag{3}$$

where ϕ is the rotation angle of the crystal and subscript i is a cube axis about which the sample is rotated. A_i, B_i, and C_i were determined by fitting the observed splitting to Eq. 3. The quadrupole coupling constant in the laboratory frame can be derived from the following equations:

$$\begin{aligned}
e^2Qq_{XX}/h &= (1/2)(A_Y - B_Y + A_Z + B_Z),\\
e^2Qq_{YY}/h &= (1/2)(A_Z - B_Z + A_X + B_X),\\
e^2Qq_{ZZ}/h &= (1/2)(A_X - B_X - A_Y + B_Y),\\
e^2Qq_{XY}/h &= e^2Qq_{YX}/h = -C_Z,\\
e^2Qq_{XZ}/h &= e^2Qq_{ZX}/h = -C_Y,\\
e^2Qq_{YZ}/h &= e^2Qq_{ZY}/h = -C_X.
\end{aligned} \tag{4}$$

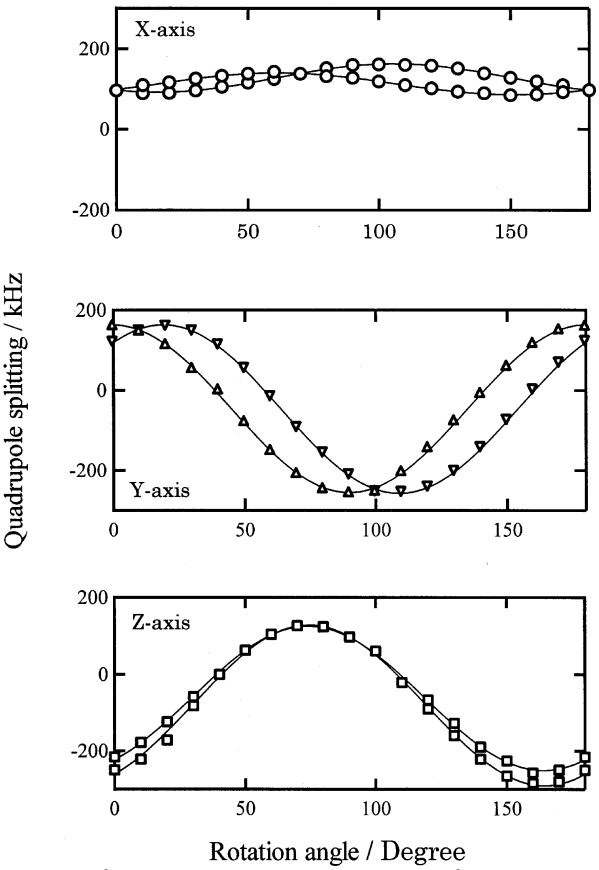

Fig. 9. ^{2}H NMR rotation pattern on $[C_5H_5N^2H]SbBr_4$ at 77 K.

The quadrupole coupling constant in the principal axis system and its orientation were determined by diagonalizing this laboratory frame tensor. The quadrupole coupling parameters, e^2Qq/h and η, were determined to be 123(1) kHz, 0.70(1) at 285 K and 191(1) kHz, 0.14(2) at 77 K. These values are in good agreement with those from the powder patterns. Although the orientation of the single crystal was arbitrarily chosen with respect to the laboratory frame, the relative orientation of the q_{zz} axis with respect to the crystal b-axis could be determined from these experiments. At Phase I the q_{zz} axis must be parallel to the b-axis due to the site symmetry of the N–^{2}H bond. However, one q_{zz} direction at 285 K split into two at 77 K, making an angle 16.8(1)° due to the twin structure. On the other hand, the rotational shift angle of the pyridinium cation, defined as the angle between the N(1)–C(3) direction and a bisector of the < Br(1)Sb(1)Br(2), was estimated to be 8.4° at 110 K. This angle, evaluated from the X-ray crystallographic data, corresponds just to one half that of the two q_{zz} axes. This suggests that the twin structure below T_{tr} is formed by clockwise and anti-clockwise rotations of the pyridinium cations.

This work was supported by a Grant-in-Aid for Scientific Research No.11694084 from the Ministry of Education, Science, Sports and Culture.

References

1 K. Yamada and T. Okuda, "Chemistry of Hypervalent Compounds," ed by K. Akiba, Wiley-VCH, New York (1999), Chap. 3.

2 D. K. Seo, N. Gupta, M. -H. Whangbo, M. Hillebrecht, G. Thiele, *Inorg. Chem.*, **1998**, 37, 407.

3 K. Yamada, T. Matsui, T. Tsuritani, T. Okuda, and S. Ichiba, *Z. Naturforsch.*, **45a**, 307 (1990).

4 K. Yamada, S. Nose, T. Umehara, T. Okuda, and S. Ichiba, *Bull. Chem. Soc. Jpn.*, **61**, 4265 (1988).

5 K. Yamada, K. Isobe, T. Okuda, and Y. Furukawa, *Z. Naturforsch.*, **49a**, 258 (1994); K. Yamada, K. Isobe, E. Tsuyama, T. Okuda, and Y. Furukawa, *Solid State Ionics*, **79**, 152 (1995).

6 K. Yamada, Y. Ohnuki, H. Ohki, and T. Okuda, *Chem. Lett.*, **1999**, 627.

7 T. A. Albright, J. K. Burdett, and M.-H. Whangbo, "Orbital Interactions in Chemistry," John Wiley & Sons, Inc. (1985), Chap. 14.

8 G. C. Pimentel and R. D. Spratley, "Chemical Bonding," Holden-Day, Inc. (1969), Chap. 7.

9 T. Okuda, K. Yamada, H. Ishihara, M. Hiura, S. Gima, and H. Negita, *J. Chem. Soc., Chem. Commun.*, **1981**, 979.

10 K. Yamada, T. Ohtani, S. Shirakawa, H. Ohki, T. Okuda and T. Kamiyama, H. Oikawa, *Z. Naturforsch.*, **51a**, 739 (1996).

11 P. T. Beurskens, G. Admiraal, G. Beurskens, W. P. Bosman, S. Garcia-Granda, R. O. Gould, J. M. M. Smits, and C. Smykalla, "PATTY" (1992). The DIRDIF program system, Technical Report of the Crystallography Laboratory, University of Nijmengen, The Netherlands.

12 "teXsan" Single Crystal Structure Analysis Software. Version 1.9, Molecular Structure Corporation, Rigaku Corporation (1998).

13 P. W. DeHaven and R. A. Jacobson, *Cryst. Struct. Commun.*, **5**, 31 (1976).